RISCOS

territorium 27 (II), 2020, 41-48

journal homepage: https://territorium.riscos.pt/numeros-publicados/

DOI: https://doi.org/10.14195/1647-7723_27-2_4

PRINCIPAL COMPONENT ANALYSIS OF C-SAR IMAGES FOR FLOOD MAPPING – SANTA FE PROVINCE, ARGENTINA*

ANÁLISE DE PRINCIPAIS COMPONENTES DE IMAGENS C-SAR PARA MAPEAMENTO DE INUNDAÇÃO – PROVÍNCIA DE SANTA FE, ARGENTINA

Jones Zamboni Graosque

Universidade Federal do Rio Grande do Sul
Programa de Pós-Graduação em Geografia (Brasil)
ORCID 0000-0002-8451-904X jones.eu@gmail.com

Laurindo Antonio Guasselli

Universidade Federal do Rio Grande do Sul
Programa de Pós-Graduação em Geografia (Brasil)
ORCID 0000-0001-8300-846X laurindo.guasselli@ufrgs.br

ABSTRACT

Flood events are phenomena associated with heavy rainfall. In Argentina, floods have high economic and social costs, including loss of human life. In this paper, principal component analysis (PCA) is used to map flood-prone areas along the Paraná river in Santa Fe, Argentina. The Sentinel-1B (S1B) images, sensor C-SAR with VH polarisation Interferometric type (IW) Ground Range Detected (GRD) with spatial resolution of 10 m, from 2016, were referenced and the PCA method was used to extract the four first principal components. The flood-affected images make it possible to accurately define the flooded area. In targets with dense vegetation, however, there is no pixel backscatter pattern. PC2 better highlighted the threshold of pixel intensity, with an accuracy of 70%, and 93% of the mapped area was shown to be flood-prone. Procedures to map floods remotely are pivotal because they can quickly obtain precise data on flood areas that may not be accessible for fieldwork or that have not yet been mapped in great detail.

Keywords: Sentinel-1, time series analysis, principal components, Argentina.

RESUMO

Inundações são associadas a chuvas intensas. Na Argentina é o evento natural que causa mais perdas econômicas, sociais e de vidas humanas. O objetivo desse trabalho é mapear a área de inundação do rio Paraná, em Santa Fe, por Análise de Componentes Principais (ACP). As imagens Sentinel-1B, sensor C-SAR, polarização VH do tipo Interferométrico (IW) *Ground Range Detected* (GRD), pixel de 10 m, ano 2016, foram referenciadas, extraindo as quatro primeiras ACP. As imagens sob efeito de inundação permitiram delimitar com precisão a área inundada. No entanto, em áreas com densidade de vegetação não há um padrão de retroespalhamento dos pixéis. A PC2 destacou melhor o limiar de intensidade dos pixéis de inundação, com uma precisão de 70%, sendo que 93% da área mapeada é suscetível à inundação. A cartografia de risco de inundação obtida a partir de sensoriamento remoto revela-se essencial, pois possibilita a obtenção de resultados rápidos e precisos das áreas de inundação, em áreas cujo trabalho de campo não seja possível ou não se encontrem disponíveis mapas detalhados das áreas atingidas.

Palavras-chave: Sentinel-1, análise temporal, principais componentes, Argentina.

* *O texto deste artigo foi submetido em 24-01-2019, sujeito a revisão por pares a 12-02-2019 e aceite para publicação em 28-03-2019.*

Introduction

Among natural disasters, floods may be the most common ones causing more destruction than any other natural hazard worldwide (Sanyal & Lu, 2004; Tingsanchali, 2012; Rahman & Thakur, 2018).

In Argentina, floods are the main natural cause for economic and social losses as well as loss of human life. In the Litoral region alone – comprising the provinces Formosa, Chaco, Missiones, Corrientes, Santa Fe, and Entre Rios – 165 people perished and almost 6,000 were injured due to fluvial flooding events between 1970 and 2004. Nearly one million people had to be evacuated, and approximately 18,000 houses were destroyed. An estimated 1.7 million head of cattle were lost, and 28 million hectares of farm land were affected (Celis, 2006). This region has already sustained substantial losses in agriculture and cattle husbandry inflicting significant damage on these sectors (Notícias Agrícolas, 2018; Correio do Brasil, 2018; Agrolink, 2018).

Flood maps of the city of Santa Fe were developed based on fieldwork and optical imaging of flooding events in 2003 and 2007 (Vallejos *et al.*, 2014). This data was paramount to devise emergency plans and protection structures for the city of Santa Fe (Fe, 2018).

However, flood maps based on optical imaging may not render the correct dimensions of the flooded area due to cloudy skies or vegetation. Some studies suggest that Synthetic Aperture Radar (SAR) sensors provide better results to detect floods than optical sensors (Hess & Melack, 1994; Townsend & Walsh, 1998; Tralli *et al.*, 2005; Clement *et al.*, 2018; Markert *et al.*, 2018).

The Global Flood Monitoring System (GFMS) provides updated maps on floods and precipitation online (Wu *et al.*, 2014). In addition, tools such as Earth Data and GFMS provide valuable and low-cost hydrological data which may contribute to flood maps and policy development (Yan *et al.*, 2015). GFMS is an efficient system that provides maps shortly after the event. The spatial resolution, however, amounts to 1 km compromising the level of detail of the flood area (Wu *et al.*, 2014). In general, the flood maps of the region of the city of Santa Fe mainly indicate how far the water proceeds in urban areas; they address potentially flooded areas in smaller communities or rural areas only secondly.

Using radar images to map floods can offset the restrictions of optical imaging. One of the most commonly applied techniques is thresholding. It is a conventional method to map non-forested areas that maximises the contrast between water and land facilitating the representation of floods in histograms (Brivio *et al.*, 2002; Malnes *et al.*, 2002; Solbø & Solheim, 2004; Rahman & Thakur, 2018).

When applied to a single image, the thresholding method may not size a flooding event precisely; however, when applied to a time series of images, it becomes increasingly accurate since even flood water covered by vegetation is detected. Considering that a greater amount of images is required to conduct the analysis and that the procedure is more complex, the maps can be more precise, especially in vertical targets such as wooded areas (Townsend, 2001 and 2002; Kandus *et al.*, 2001; Solbø & Solheim, 2004).

Principal Component Analysis (PCA) permits processing images with a greater number of spectrum bands and obtaining information from multi-temporal data (Crosta, 1992; Sato *et al.*, 2011). PCA provides a new set of variables, simplifies the description of the data set, and analyses the structure of the observations and variables (Abdi & Williams, 2010). It proves to be a promising method to detect the dynamics and changes in land cover such as in case of floods (Dutsenwai *et al.*, 2016).

When mapping floods on the basis of remote sensing tools, the more comprehensive the time series of images in the PCA is, the better the results are as water can be mapped even in vertical target areas, such as densely vegetated areas (Solbø & Solheim, 2004; Santoro *et al.*, 2015; Graosque, 2018). Thus, this paper aims at mapping flood areas employing Principal Component Analysis in the area surrounding the city of Santa Fe, Argentina.

Area of study

The area of study encompasses a section of the Paraná river which divides the two Argentinian provinces Santa Fe and Entre Ríos and borders on the cities of Santa Fe and Paraná. In the area, the floodplain comprises urban and rural areas resulting in urban parts of Santa Fe being flood-prone.

The analysed region (fig. 1) was classified as urban areas, rural areas, humid areas or wooded areas, in addition to permanent water bodies such as the Paraná river (Benzaquén & Argentina, 2013).

Methodology

Radar images of the satellite Sentinel -1B (S1B) from 2016 were analysed to map flood-prone areas in the region. The Synthetic Aperture Radar (SAR) images are C-band, Vertical Horizontal (VH) polarised and were acquired in Interferometric Wide Swath (IW) mode. The softwares SNAP and ArcMap 10.2 were used to process the images.

The table outlines the 2016 images and the respective level of the Paraná river in the city of Santa Fe. The alert level for major flooding of this river in Santa Fe is 5.3 metres (Table I). The river's average level is 3.6 metres (Centro de Informaciones Meteorológicas, 2018).

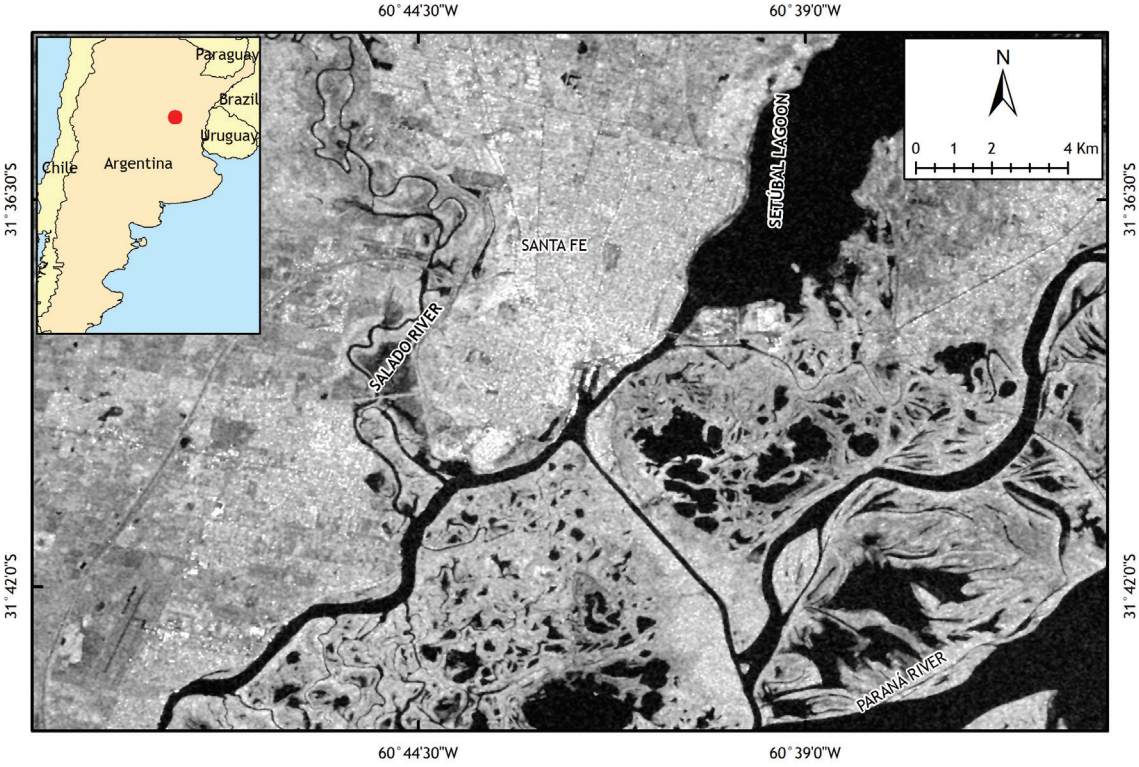

Fig. 1 - Area of study. Section of the Paraná river and the city of Santa Fe in Santa Fe province, Argentina (Data source: Sentinel 1 C-SAR image from 10th October 2016. Coordinate system: GCS WGS84).

Fig. 1 - *Área de estudo, trecho do rio Paraná e cidade de Santa Fe, na província de Santa Fe, Argentina (Fonte dos dados: Imagem SAR-C Sentinel 1 do dia 10 de outubro de 2016.Sistema de coordenadas: GCS WGS84).*

Table I - List of images used in the Principal Component Analysis.

Tabela I - *Lista das imagens utilizadas na Análise de Principais Componentes.*

Image	Date	Type	Polarisation	Mode	Water level (in m)
S1B	07/02/2016	GRD	VH	IW	6.46
S1B	26/03/2016	GRD	VH	IW	5.92
S1B	19/04/2016	GRD	VH	IW	6.38
S1B	10/09/2016	GRD	VH	IW	3.47
S1B	28/09/2016	GRD	VH	IW	2.99
S1B	10/10/2016	GRD	VH	IW	2.79
S1B	22/10/2016	GRD	VH	IW	3.02
S1B	03/11/2016	GRD	VH	IW	3.51
S1B	15/11/2016	GRD	VH	IW	3.54
S1B	27/11/2016	GRD	VH	IW	3.21
S1B	09/12/2016	GRD	VH	IW	3.02
S1B	21/12/2016	GRD	VH	IW	3.15

Data source: Sentinel-1 imagery and Meteorological Information Center, 2018.

Fonte dos dados: Imagens Sentinel-1 e Centro de Informaciones Meteorológicas, 2018.

Prior to the Principal Component Analysis, the images were calibrated, filtered (speckle), and complemented with orbital information and terrain correction. Furthermore, all images were georeferenced based on the 22nd October 2016 image using 2,000 reference points automatically extracted by the software SNAP. The same software generated the principal component images, which include, among others, one image without and another with the effects of floods, both after pre-processing (fig. 2).

The validation of the flooded area was restricted to the flood maps developed for the city of Santa Fe in 2003 (International Disasters Charter, 2019) since fieldwork was not feasible. For comparison purposes, the thresholding method was applied to the image with the highest water level, namely the one from 7th February 2016 (Graosque, 2018).

Results

Targets with variations in pixel intensity between images with and without floods were used to delineate the flooded areas. The area covered by water varies according to the image sequence facilitating the identification of flooded areas while averting the risk of misinterpreting permanent water bodies.

The principal component image that represents the flooded areas best is PC 2. The images from February, March and April (images with floods) contribute to the principal component (Table II).

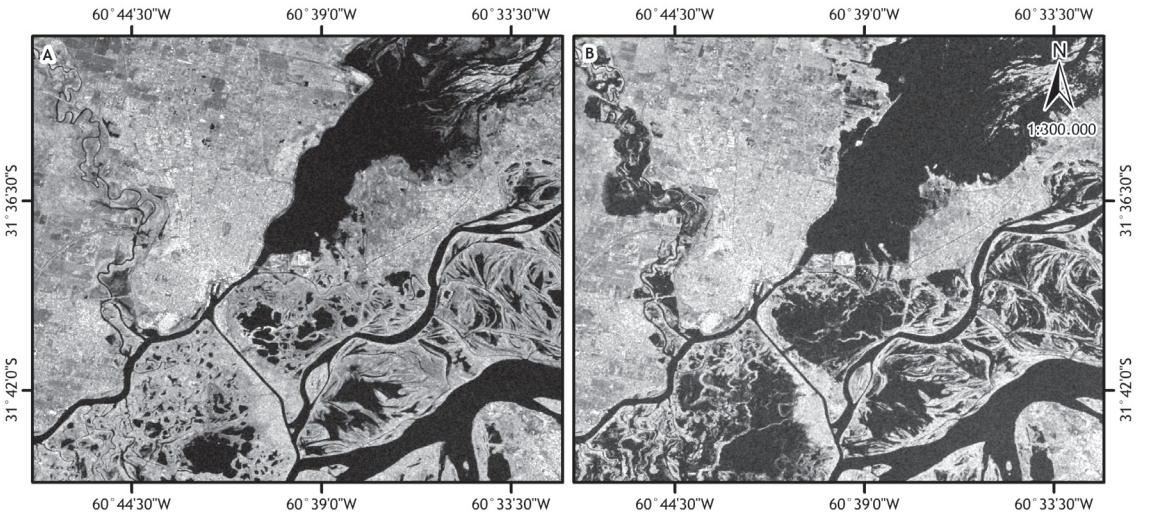

Fig. 2 - Radar image from 10 October 2016 (A); Radar image from 7 February 2016 (B).

***Fig. 2 -** Imagem de radar do dia 10 de outubro de 2016 (A); Imagem de radar do dia 7 de fevereiro de 2016 (B).*

Table II - Principal component contribution generated by analysing radar image time series (Flood dates highlighted in blue).

***Tabela II -** Contribuição das Principais Componentes, geradas pela análise temporal de imagens de radar (Datas dos eventos de inundação destacados em azul).*

Image	PC 1	PC 2	PC 3	PC 4
7th Feb	0.2846	0.3587	0.1745	-0.4757
26th Mar	0.2958	0.4806	-0.1146	0.0640
19th Apr	0.3260	0.5725	-0.1586	0.0510
10th Sep	0.2582	-0.0109	0.5465	0.1677
28th Sep	0.2790	-0.1438	0.5238	0.0370
10th Oct	0.2787	-0.172	0.2585	0.1909
22nd Oct	0.2989	-0.147	-0.1186	0.3478
3rd Nov	0.2969	-0.0963	-0.1601	0.3607
15th Nov	0.2898	-0.2033	-0.1579	-0.0466
27th Nov	0.3096	-0.1962	-0.4543	0.1372
9th Dec	0.2686	-0.2508	-0.0973	-0.3906
21st Dec	0.2705	-0.297	-0.1028	-0.5255

In PC 2 the dark-coloured pixels indicate major variations; those in light grey or white suggest no major pixel changes. The Setubal lagoon is a prime example of a permanent water body represented in light grey (fig. 3-B). Around the water bodies, however, dark areas appear indicating changes in pixel intensity between the twelve images. These dark areas are mainly located in proximity to the Salado river, to humid areas, and along the shore of the Setubal lagoon.

Image PC 1 concentrates 97 % of the eigenvalues and represents the pixels all images share. All images maintain a uniform contribution since the features of the targets are continuous throughout the dates (Henebry, 2014). PC 1 is very similar to the image of the area of study before applying the method making it difficult to differentiate between water pixels and non-water pixels (fig. 3-A). Consequently, PC 1 is not ideal for flood evaluation.

PC 2, 3 and 4 emphasise information that is less common compared to PC 1. Among these, PC 3 and 4 show variations in image contributions and highlight specific targets such as rural areas (fig. 3-C and D). These two PCs combined represent 0.8 % of the eigenvalues. Moreover, the main contributing images for these two PCs are images with and without floods which drastically reduces the chances of identifying a specific threshold for flood water.

PC 2 and 3 concentrate the greatest water body variation (Goméz-Palacios *et al.*, 2017). PC 2, however, contains three times more eigenvalues than PC 3 qualifying it as the main PC for flood analysis. Furthermore, PC 2 illustrates how the images that contribute most eigenvalues are exactly those dated to events with water levels above the alert level (5.3 metres) indicating a variation in flood-related pixels in this principal component.

PC 2 contributed 1.4 % of the eigenvalues, and targets with the highest variation show dark pixels while targets with little variation are represented by lighter pixels (fig. 3-B). The Setubal lagoon is a permanent water body with minimum pixel variation. Consequently, this water body can be consulted to define the threshold for what is water and what is not. Pixel intensity may vary in urban and rural targets; however, urban targets need to be disregarded since this method and the applied tools are inappropriate to map floods in such targets (Solbø & Solheim, 2004; Henry *et al.*, 2006). Regarding vegetation, the crop and the season of every area must be taken into consideration (Santoro & Wegmüller, 2014).

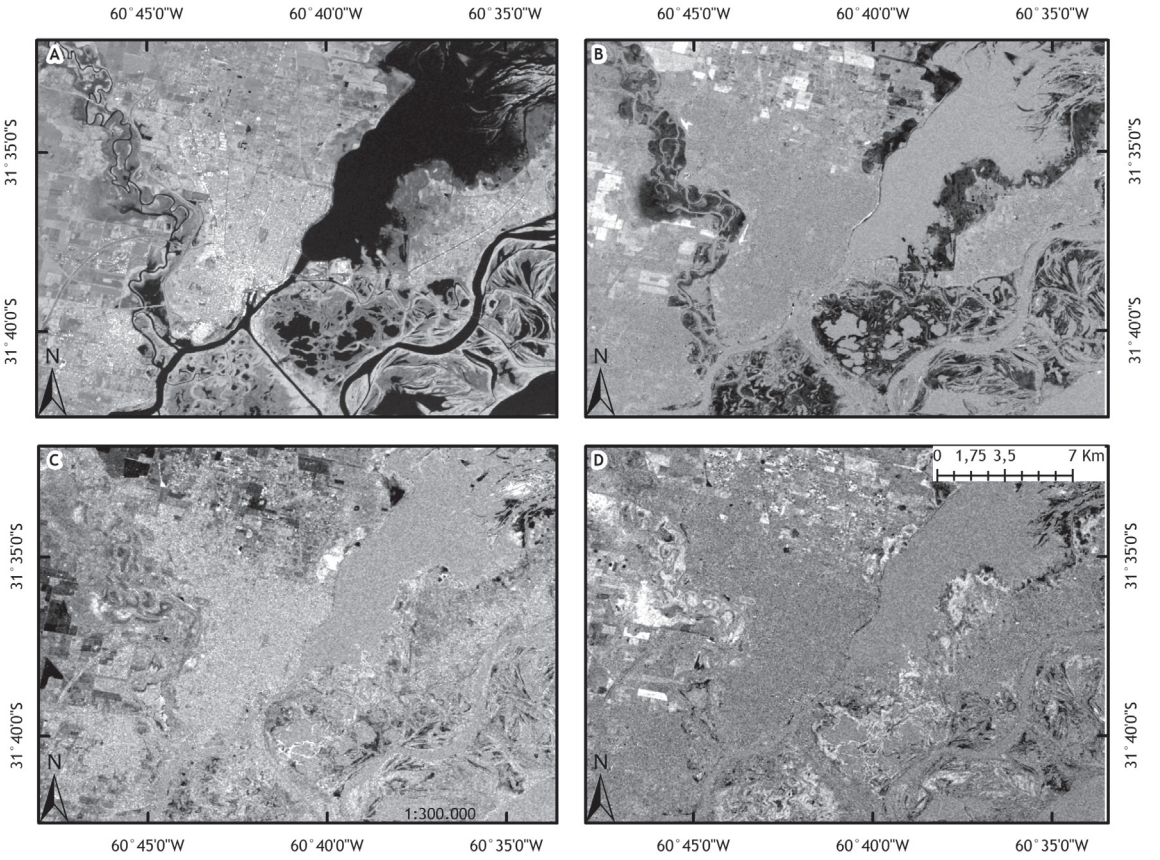

Fig. 3 - Principal component images in the area of the city of Santa Fe, Argentina, obtained by analysing a time series of VH polarised C-SAR images from January to December 2016: (A) PC 1; (B) PC 2; (C) PC 3 and (D) PC 4.

Fig. 3 - *Imagens das Componentes Principais na área da cidade de Santa Fe, Argentina, obtidas por análise temporal de imagens SAR banda C e polarização VH no período de Janeiro a Dezembro de 2016: (A) PC1; (B) PC2; (C) PC3 e (D) PC4.*

The flood areas mapped in PC 2 are mainly located in humid target areas where vertical vegetation is lower (Wu *et al.*, 2014). Wooded and rural areas, however, were also partially identified as flood areas. Although vegetation cover prevents the identification of water depth in these targets, the pixel intensity varies between the images with and without floods. PC 2 shows the pixel variation in flood targets best (fig. 4).

The flood map from April 2003 (International Disasters Charter, 2019) was used to validate the results surrounding the city of Santa Fe including areas of the Salado river (fig. 5). In comparison with this map, the use of PC 2 achieved an accuracy of 54.37 %. Based on the results, 93.03 % of the mapped area is considered flood-prone. In less urbanised areas comprising more wooded and humid areas, the accuracy was calculated based on the flood area developed by Graosque (2018) because Argentina floods (2019) only mapped the city of Santa Fe. In wooded and humid areas, the PC 2 method achieved an accuracy of 70.26 %.

The flood area could be mapped with only one image (fig. 4-B); however, the comparison with the technique of Principal Component Analysis shows that the thresholding method with a single image did not fully map flood-prone areas (fig. 4). Technically, PCA also uses a threshold to identify water and non-water which is, however, defined by multiple images. The observed target threshold using a single image was -22.5 [db] while it was 0.0 [db] using PCA in PC 2 (Goméz-Palacios *et al.*, 2017; Graosque, 2018). The change in threshold values is due to the fact that in PC 2 the image basically distinguishes between pixels that varied and those that did not undergo any variation.

In addition to diverging thresholds, the differences between the methods using a time series of images and those using a single image are reflected in vertical targets such as vegetation. Mapping efforts applying the thresholding method with a single image are only recommended for flat areas (Malnes *et al.*, 2002; Solbø & Solheim, 2004; Tuan & Duong, 2009). Analysing a time series of multiple images and hence identifying variations in pixel intensity makes it possible to map water in targets with trees, for example.

Since these tools are inappropriate to analyse floods in urban areas (Solbø & Solheim, 2004), urban Santa Fe and Santo Tomé were excluded from mapping (fig. 5).

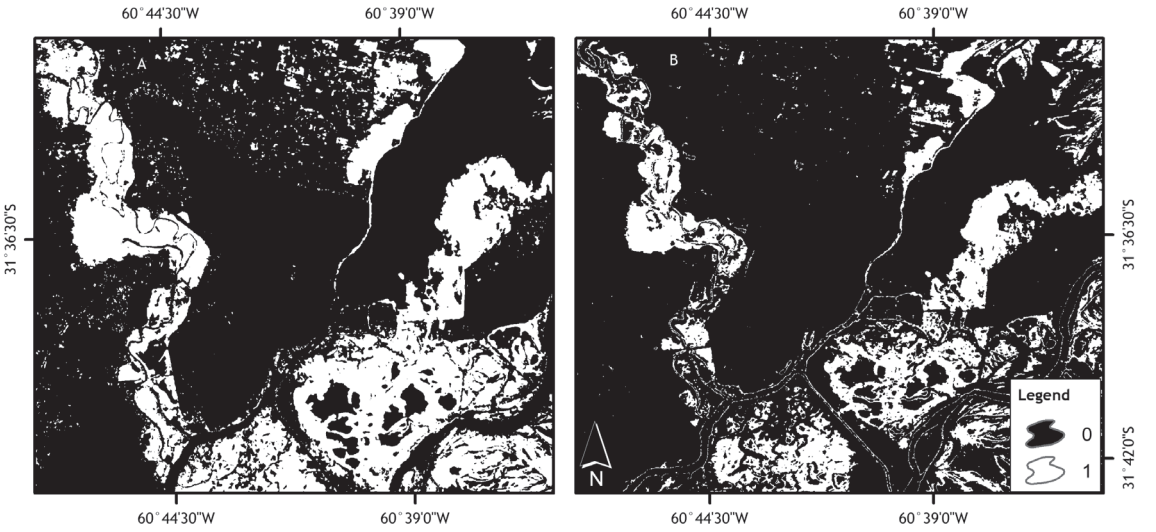

Fig. 4 - Comparison of the flood areas obtained by distinct remote sensing techniques using C-band SAR images: 1) flood water; 0) non-flooded area. (A) Flood area obtained by Principal Components 2 (PC 2) using the Sentinel-1B image series available for 2016; (B) Flood area developed by thresholding method using only the Sentinel-1B image from 7 February 2016.

Fig. 4 - *Comparação das manchas de inundação obtidas com técnicas distintas de sensoriamento remoto utilizando imagens SAR com banda C: 1) área inundada; 0) área não inundada. (A) área de inundação obtida por análise das Componentes Principais 2 (PC2) utilizando a série de imagens do Sentinel-1B disponíveis para o ano de 2016; (B) área de inundação elaborada pelo método de limiarização utilizando apenas a imagem do Sentinel-1B do dia 7 de fevereiro de 2016.*

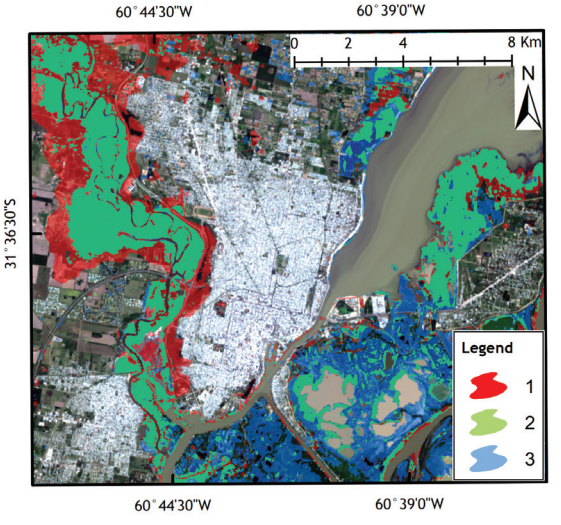

Fig. 5 - Flood areas based on the Principal Component Analysis using a time series of images: 1) Flood map from April 2003; 2) Common flood area in flood map from April 2003 and the flood map based on PCA method; 3) Flood map based on PCA method. The flood mask is superimposed on a 30-metre resolution Landsat-8 image from 3 October 2016.

Fig. 5 - *Áreas de inundação obtidas a partir da série temporal por Análise de Componentes Principais:1) Mapa de inundação de abril de 2003; 2) Área de inundação representada nos mapas de inundação de abril de 2003 e no mapa de inundação elaborado pelo método de ACP; 3) Mapa de inundação baseado no método de ACP. A área de inundação foi sobreposta à imagem Landsat - 8 com resolução de 30 metros referente ao dia 03 de outubro de 2016.*

Conclusions and recommendations

Principal Component Analysis proves to be a viable option to map flood areas remotely because in addition to the precision of the result, the threshold between water and non-water is identified more precisely for horizontal as well as vertical targets. Only PCA (mainly in PC 2) permits to evaluate in which images the water level was elevated; however ideally, this information should be available before applying the method because the images that are expected to provide a major contribution to PC 2 would already be known. Measuring water levels in the field could provide such information.

Another distinctive feature is, however, that the method is not applicable to map floods in urban areas. For this reason, the urban areas of Santa Fe and Santo Tomé were not included in the mapping process.

Moreover, the use of PCA to map floods in rural areas may show divergence in the final result due to the types of crops and the season during which the images were taken. In this case, information on the area is required for the flood analysis.

References

Abdi, H., & Williams, L. J. (2010). Principal component analysis: Principal component analysis. *Wiley Interdisciplinary Reviews: Computational Statistics*, 2(4), 433–459. DOI: https://doi.org/10.1002/wics.101

Agrolink. (2018). *Argentina pode perder 10% da safra de soja com incêndios e inundações*. Accessed 30th December 2018, on https://www.agrolink.com.br/agrotempo/noticia/argentina-pode-perder-10--dasafra-de-soja-com-incendios-e-inundacoes_368135.html

ARGENTINA FLOODS - ACTIVATIONS - INTERNATIONAL DISASTERS CHARTER. (2019). Accessed 16th January 2019, on https://disasterscharter.org/web/guest/activations/-/article/argentina-floo-6

Benzaquén, L., & Argentina (Orgs.). (2013). *Inventario de los humedales de Argentina: sistemas de paisajes de humedales del corredor fluvial Paraná-Paraguay* (1a edición). Buenos Aires: Secretaría de Ambiente y Desarrollo Sustentable de la Nación.

Brivio, P. A., Colombo, R., Maggi, M., & Tomasoni, R. (2002). Integration of remote sensing data and GIS for accurate mapping of flooded areas. International *Journal of Remote Sensing*, 23(3), 429–441. DOI: https://doi.org/10.1080/01431160010014729

Celis, A. (2006). Desastres en la Región Litoral de Argentina: 1970-2004. *PAMPA*, (2), 85–109. DOI: https://doi.org/10.14409/pampa.v1i2.3132

CENTRO DE INFORMACIONES METEOROLÓGICAS (2018). Altura de la Cuenca del Paraná. Accessed 10th June 2018, on http://fich.unl.edu.ar/cim/alturas-rio-parana

Clement, M. A., Kilsby, C. G., & Moore, P. (2018). Multi-temporal synthetic aperture radar flood mapping using change detection: Multi-temporal SAR flood mapping using change detection. J*ournal of Flood Risk Management*, 11(2), 152–168. DOI: https://doi.org/10.1111/jfr3.12303

CORREIO DO BRASIL (2018). Argentina pede créditos para reconstruir cidade inundada. Accessed 30th December 2018, on https://arquivo.correiodobrasil.com.br/argentina-pede-creditos-para-reconstruir-cidade-inundada/

Crosta, A. P. (1992). Processamento Digital de Imagens de Sensoriamento Remoto. IG/UNICAMP, Campinas, SP, 170 p.

Dutsenwai, H. S., Ahmad, B. B., Mijinyawa, A., & Tanko, A. I. (2016). 37 Fusion of SAR images for flood extent mapping in northern peninsula Malaysia. *International Journal of Advanced and Applied Sciences*, 3(12), 37–48. DOI: https://doi.org/10.21833/ijaas.2016.12.006

ESA/CCI viewer. (2015). Land cover and conditions of the Climate Change Initiative project. Accessed 18th May 2017, on http://maps.elie.ucl.ac.be/CCI/viewer/index.php

Fe, G. de S. (2018). *Gobierno de santa fe - traslado de animales por la emergencia hídrica*. Accessed 21st December 2018, on https://www.santafe.gob.ar/index.php/web/content/view/full/159155/(subtema)/93794

Gómez-Palacios, D., Torres, M. A., Reinoso, E. (2017). Flood mapping through principal component analysis of multitemporal satellite imagery considering the alteration of water spectral properties due to turbidity conditions. *Geomatics, Natural Hazards and Risk*, 8(2), 607–623. DOI: https://doi.org/10.1080/19475705.2016.1250115

Graosque, J. Z. (2018). *Mapeamento das áreas de inundação utilizando imagens C-SAR e SRTM , nas províncias de Santa Fé e Entre Ríos, Argentina*. Universidade Federal do Rio Grande do Sul. Instituto de Geociências. Programa de Pós-Graduação em Geografia, Porto Alegre. Accessed on http://hdl.handle.net/10183/179578

Henebry, M. G. (2014). *Advantages of principal components analysis for land cover segmentation from SAR image series*. Accessed 22nd December 2018, on http://earth.esa.int/workshops/ers97/papers/henebry3/index.html

Henry, J. -B., Chastanet, P., Fellah, K., & Desnos, Y. -L. (2006). Envisat multi-polarized ASAR data for flood mapping. *International Journal of Remote Sensing*, 27(10), 1921–1929. DOI: https://doi.org/10.1080/01431160500486724

Hess, L., Melack, J. M. (1994). Mapping wetland hydrology and vegetation with Synthetic Aperture Radar. International *Journal of Ecology and Environmental Sciences*, v. 20, 197–205.

Kandus, P., Karszenbaum, H., Pultz, T., Parmuchi, G., & Bava, J. (2001). Influence of flood conditions and vegetation status on the radar backscatter of wetland ecosystems. *Canadian Journal of Remote Sensing*, 27(6), 651–662. DOI: https://doi.org/10.1080/07038992.2001.10854907

Malnes, E., Guneriussen, T., Høgda, K. A. (2002). Mapping of Flood-area by Radarsat in Vannsjø, Norway. I*n Proc. International Symposium on Remote Sensing of Environment*, Buenos Aires.

Markert, K. N., Chishtie, F., Anderson, E. R., Saah, D., & Griffin, R. E. (2018). On the merging of optical and SAR satellite imagery for surface water mapping applications. *Results in Physics*, 9, 275–277. DOI: https://doi.org/10.1016/j.rinp.2018.02.054

NOTICIAS AGRICOLAS (2018). Quase 3,5 milhões de hectares estão afetados pelas inundações na Argentina;... - Notícias Agrícolas. Accessed 30th December 2018, on https://www.noticiasagricolas.com.br/noticias/soja/185742-quase-35-milhoes-de-hectares-estao-afetados-pelas-inundacoes-na-argentina-saiba-o-que-aconteceu-ate.html

Rahman, M. R., & Thakur, P. K. (2018). Detecting, mapping and analysing of flood water propagation using synthetic aperture radar (Sar) satellite data and GIS: A case study from the Kendrapara District

of Orissa State of India. *The Egyptian Journal of Remote Sensing and Space Science*, 21, S37–S41. DOI: https://doi.org/10.1016/j.ejrs.2017.10.002

Santa fe mapas | el mapa interactivo de la ciudad de santa fe. (2018). Accessed 21st December 2018, on http://muniweb1.santafeciudad.gov.ar/santafemapas/#

Santoro, M., & Wegmuller, U. (2014). Multi-temporal synthetic aperture radar metrics applied to map open water bodies. *IEEE Journal of Selected Topics in Applied Earth Observations and Remote Sensing*, 7(8), 3225–3238. DOI: https://doi.org/10.1109/JSTARS.2013.2289301

Santoro, M., Wegmüller, U., Lamarche, C., Bontemps, S., Defourny, P., & Arino, O. (2015). Strengths and weaknesses of multi-year Envisat ASAR backscatter measurements to map permanent open water bodies at global scale. *Remote Sensing of Environment*, 171, 185–201. DOI: https://doi.org/10.1016/j.rse.2015.10.031

Sanyal, J., & Lu, X. X. (2004). Application of remote sensing in flood management with special reference to monsoon asia: a review. *Natural Hazards*, 33(2), 283–301. DOI: https://doi.org/10.1023/B:NHAZ.0000037035.65105.95

Sato, L. Y., Shimabukuro, Y. E., Kuplich, T. M. (2011). Uso da análise por componentes principais na avaliação da mudança da cobertura florestal da Floresta Nacional do Tapajós. *Anais XV Simpósio Brasileiro de Sensoriamento Remoto - SBSR*, Curitiba, PR, Brasil, INPE, 6696 p.

Solbø, S., Solheim, I. (2004). Towards Operational Flood Mapping with Satellite SAR. Norut Information Technology AS. Tromsø Science Park, N-9291 Tromsø, Norway. *Proc. of the 2004 Envisat & ERS Symposium*, Salzburg, Austria.

Tingsanchali, T. (2012). Urban flood disaster management. *Procedia Engineering*, 32, 25–37. DOI: https://doi.org/10.1016/j.proeng.2012.01.1233

Townsend, P. A. (2002). Relationships between forest structure and the detection of flood inundation in forested wetlands using C-band SAR. *International Journal of Remote Sensing*, 23(3), 443–460. DOI: https://doi.org/10.1080/01431160010014738

Townsend, P. A. (2001). Mapping seasonal flooding in forested wetlands using multitemporal Radarsat SAR. *Photogrammetric Eng. Remote Sensing*, v. 67(7), p.857864.

Townsend, P. A., & Walsh, S. J. (1998). Modeling floodplain inundation using an integrated GIS with radar and optical remote sensing. *Geomorphology*, 21(3–4), 295–312. DOI: https://doi.org/10.1016/S0169-555X(97)00069-X

Tralli, D. M., Blom, R. G., Zlotnicki, V., Donnellan, A., & Evans, D. L. (2005). Satellite remote sensing of earthquake, volcano, flood, landslide and coastal inundation hazards. *ISPRS Journal of Photogrammetry and Remote Sensing*, 59(4), 185–198. DOI: https://doi.org/10.1016/j.isprsjprs.2005.02.002

Tuan, T. A., & Duong, N. D. (2009). Flood Monitoring Using ALOS/PALSAR Imagery . In *TS 3E - Disaster Risk Management: Approaches and Consequences* . Hanoi, Vietnam: Spatial Data Serving People: Land Governance and the Environment.

Vallejos, O., Matharán, G., Marichal, M. E. (2014). Las inundaciones en la ciudad de Santa Fe, Argentina, vistas desde una perspectiva CTS. *Revista Iberoamericana de Ciencia, Tecnología y Sociedad*, n.° 25, vol. 9, 147-180.

Wu, H., Adler, R. F., Tian, Y., Huffman, G. J., Li, H., & Wang, J. (2014). Real-time global flood estimation using satellite-based precipitation and a coupled land surface and routing model. *Water Resources Research*, 50(3), 2693–2717. DOI: https://doi.org/10.1002/2013WR014710

Yan, K., Di Baldassarre, G., Solomatine, D.P., and Schumann, G.J-P. (2015). A review of low-cost space-borne data for flood modelling: topography, flood extent and water level. *Hydrol. Process.*, 29, 3368– 3387. DOI: https://doi.org/10.1002/hyp.10449